

Investigation of particle packing in model pharmaceutical powders using X-ray microtomography and discrete element method

Xiaowei Fu ^{a,*}, Meenakshi Dutt ^a, A. Craig Bentham ^b, Bruno C. Hancock ^c,
Ruth E. Cameron ^a, James A. Elliott ^a

^a *Pfizer Institute for Pharmaceutical Materials Science, Department of Materials, Science and Metallurgy, University of Cambridge, Pembroke Street, Cambridge, CB2 3QZ, UK*

^b *Pfizer Ltd, Sandwich, Kent, CT13 9NJ, UK*

^c *Pfizer Ltd, Groton, CT 06340, USA*

Received 8 April 2005; received in revised form 1 May 2006; accepted 16 June 2006

Available online 29 June 2006

Abstract

This paper outlines a novel technique, based on combination of modern desktop X-ray microtomography, quantitative image processing and computer simulation using the discrete element method (DEM), to investigate randomly packed particles in an attempt to model the process of pharmaceutical tablet manufacture by powder compaction. The systems studied include glass ballotini and spheroidal micronised cellulose (Celphe), all with typical particle sizes between 180 and 300 μm . We demonstrate that X-ray microtomography (XMT) and DEM can reproduce the structure of real packing systems in three-dimensions and have the potential for further investigation of pharmaceutical processes by both modelling and experimental study. This was achieved by generating packing systems using DEM simulations that are consistent with the structural measurements made by XMT on real packed powders via the comparison of their radial distribution functions (RDFs). These results have been validated by direct volume measurements, and scanning electron microscopy (SEM) observations in terms of particle morphologies and size distribution. The result is a significant step forward for the quantitative analysis of model systems for pharmaceutical powders.

© 2006 Elsevier B.V. All rights reserved.

Keywords: X-ray microtomography; Packing; 3D imaging; Discrete element method

1. Introduction

The packing of pharmaceutical powders is an issue of great concern to industry, because the packing structure influences powder compaction and powder flow directly, which must be controlled during tablet manufacture in order to produce a high quality product. The packing structures of spheres or other regular shapes can be generated by computer simulation models, such as the discrete element method (DEM), molecular dynamics method (MD) or computational fluid dynamics technique (CFD), as reviewed in [1–3]. A variety of experimental measurements have also been employed to investigate

packing structures such as mechanical disassembly approaches [4,5], X-ray radiography [6,7], scanning confocal microscopy [8,9], magnetic resonance imaging (MRI) [10–12] and X-ray microtomography [13–17]. Among these experimental techniques, X-ray microtomography especially the recently developed Desktop X-ray microtomography, has been regarded as a robust technique and drawn most attention in this field, due to its high spatial resolution, ease of use and ability to acquire three-dimensional information.

X-ray microtomography is a non-destructive imaging technique that can produce 3D images of materials with a voxel (volume pixel) size of around several micrometers cubed, allowing the visualisation of internal and microstructural details with different X-ray absorbencies. The intensity values associated with the different features of an XMT image are determined by

* Corresponding author. Tel.: +44 1223 767059; fax: +44 1223 767063.
E-mail address: xf206@cam.ac.uk (X. Fu).

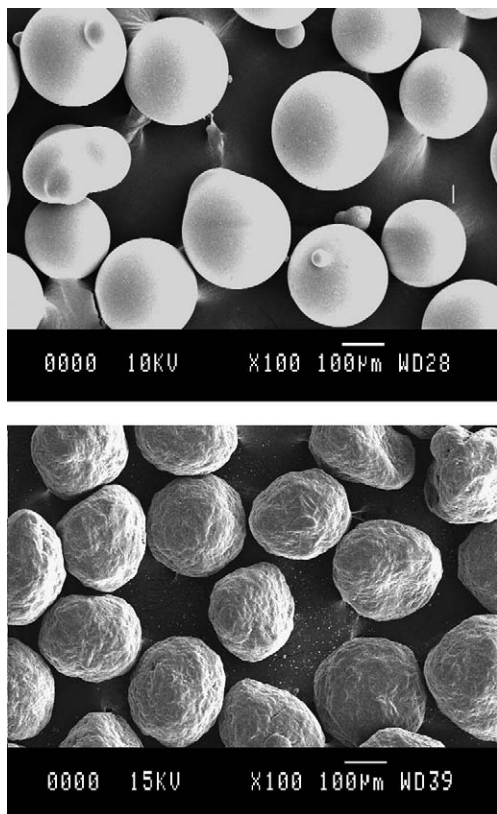


Fig. 1. Morphology of (a) polydisperse glass ballotini spheres (mean size of 250 μm) and (b) Celphere (cellulose spheres) as observed by SEM.

the X-ray transmission measured by an X-ray detection system, which is dependent on the material's atomic mass and the energy of X-rays [18,19].

In this study, we combine a 3D analysis of X-ray microtomography (XMT) and the discrete element method (DEM) in order to investigate the packing of model systems for pharmaceutical powders. A SkyScan-1072 high-resolution desktop XMT system is used, which offers a maximum spatial resolution of the order of several micrometers. A 3D watershed-based image processing algorithm was employed in the analysis of the XMT data in order to determine the size, shape and position of each individual particle within a sample. The particle size information for all the particles in a sample was then fed into DEM models to reproduce the packing. Along with bulk measurements such as the packing fraction, the internal packing structure of multi-particle systems can be quantified by the radial distribution function (RDF).

In this paper, we present investigations for nearly spherical glass ballotini and spheronised microcrystalline cellulose particles (Celphere) with a typical particle size of 180–300 μm . This work is currently being extended to study more complex powder mixtures. It should be emphasised that these systems are not intended to correspond directly to formulations used in the pharmaceutical industry, rather they consist of materials with well-characterised particle size and shape distributions which makes them more suitable for quantitative analysis by XMT.

2. Experiments on 3D particle packings

2.1. Systems studied

Ballotini glass spheres (180–300 μm ; Potters Industries, UK) and spherical microcrystalline cellulose (Celphere CP-203, Asahi Kasei Corp, Japan) were selected for characterisation (Fig. 1). All spheres were sieved to sizes of 180–212 μm or 212–300 μm (Endecotts Ltd, UK), which gave samples of particles an average particle size of around 200 or 250 μm , respectively. Sieve pairs were placed in a receiver on a sieve shaker (Retsch GmbH, Germany) for 30 min, and the process was repeated to ensure a significant output of material. The particle sizes selected are representative of those found in pharmaceutical powder blends [20], and are highly suitable for visualization by XMT. For imaging experiments, glass and cellulose spheres were poured into a borosilicate glass capillary tube of diameter 3.0 mm using a paper funnel. The tubes were then filled to a height of approximately 2 cm before being sealed with a Bunsen flame. Using this experimental set-up, the number of particles measured was about 2000, with both packing depth and width of 15–20 particles in each acquisition by XMT (Fig. 2).

2.2. Image acquisition and reconstruction

During the image acquisition process by XMT, all reconstructions used a voxel size of 5 μm , which is close to the maximum spatial resolution of the instrument. The X-ray parameters, such as voltage, filter and exposure time, were optimised with reference to the systems analysed in order to obtain the best image contrast. The images were acquired at 50 kV using a 0.5 mm diameter aluminium filter, a 5 μm pixel size, 0.23° angle step (*i.e.* 824 2D radiographs per 180° rotation) and 4-frame averages per acquired radiograph. A cone-beam accusation was selected and cone-beam volumetric reconstruction (Feldkamp algorithm) [21] was employed for image reconstruction.

Apart from optimisation of suitable parameters during image acquisition, extensive corrections of the resulting image were

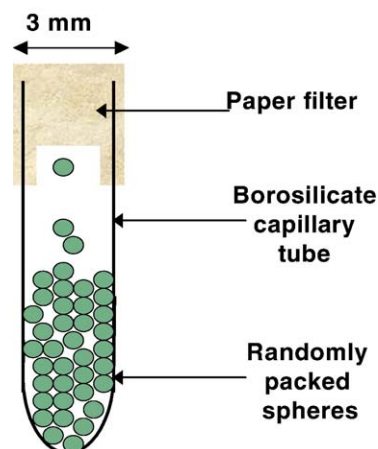


Fig. 2. Sample preparation for XMT imaging of randomly packed spheres.

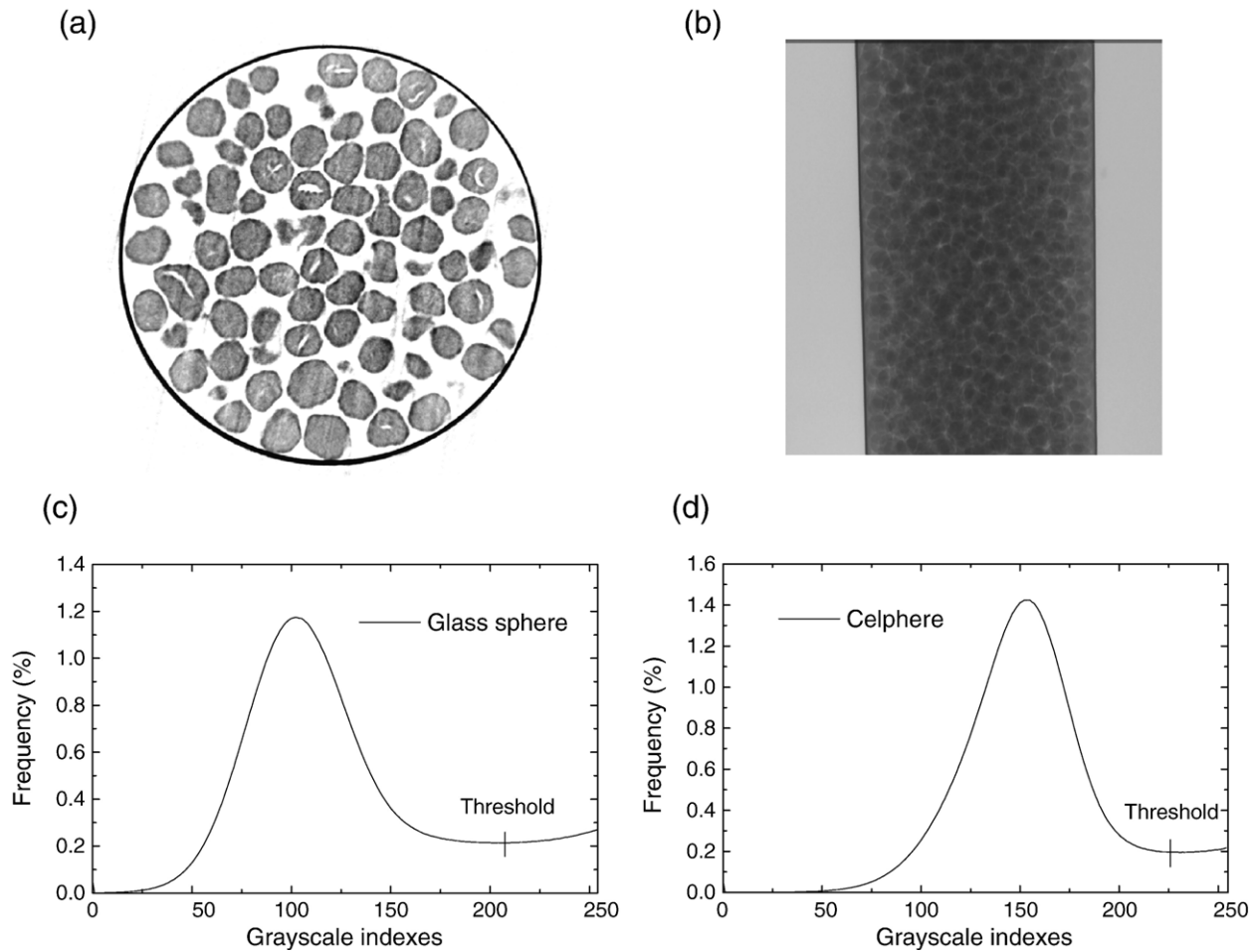


Fig. 3. (a) X-ray tomographic radiograph and (b) reconstructed cross-sectional image of Celphere particle packing, volumetric histogram of greyscales within glass sphere (c) and Celphere (d).

always necessary during image reconstruction so as to minimize a variety of artefacts, including misalignment of the sample rotation axis, beam hardening and ring artefacts. During the image reconstruction process, the beam hardening correction parameter was set to 40–60%, depending upon the individual samples. The

reconstructed images and radiograph of Celphere were shown in Fig. 3a, b. Each original reconstructed image contained 1024×1024 pixels and is displayed in 256-level greyscale. The volumetric intensity frequency histogram of greyscales within glass sphere and Celphere were shown in Fig. 3c, d respectively.

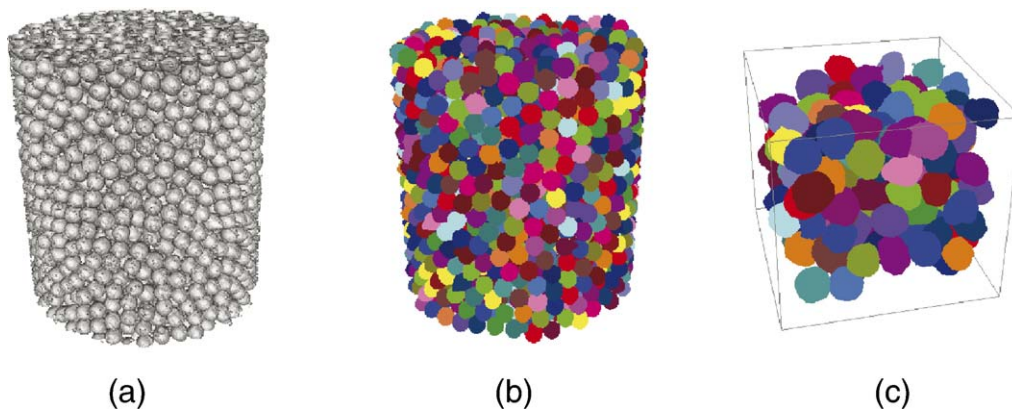


Fig. 4. (a) 3D XMT reconstructed images showing randomly packed monodisperse glass spheres; (b) 3D objects acquired from image segmentation on (a); and (c) a magnified part of packed polydisperse Celphere particles to show morphologies of particles, with particle size of 150–300 μm . The uniquely identified particles (in this case, spheres) are shown with different greyscales.

Table 1
Digital information of position, size and shape of polydisperse glass spheres obtained by XMT and image processing

Particle Index	CMS.X (μm)	CMS.Y (μm)	CMS.Z (μm)	Surface area ($10^5 \mu\text{m}^2$)	Volume ($10^6 \mu\text{m}^3$)	Diameter (μm)	Sphericity
1	1606.38	503.04	424.38	3.74	10.21	269.18	0.772
2	1529.72	1269.72	383.12	2.62	6.50	231.54	0.895
3	2111.38	1677.07	394.19	2.42	5.58	220.04	0.866
4	1105.14	2849.97	398.71	2.83	6.49	231.41	0.755
5	358.08	1160.61	407.53	2.87	6.98	237.10	0.805
6	2406.15	2385.78	419.67	2.87	7.01	237.51	0.828
7	1074.89	398.68	433.03	2.34	5.03	212.57	0.792
8	1361.21	2215.56	413.46	2.73	6.76	234.59	0.885
9	579.68	2447.99	419.21	3.08	8.01	248.19	0.861
10	1332.59	602.43	458.77	3.41	9.30	260.95	0.871

CMS.X, CMS.Y and CMS.Z stand for three coordinates of centre of masses of particle in 3D space.

Surface area is a count of the number of occurrences of a voxel in the region that is 6-way adjacent to a voxel not in the region.

Volume is the calibrated volume of the 3D object.

Sphericity is defined as $(36\pi \text{Volume}^2)/(\text{Crofton_surface_area}^3)$ (see Aphelion library), and equal to 1.0 for a perfect sphere.

Sphericity is 1.0 for a perfect sphere.

2.3. Extension of watershed-based segmentation to 3D packings

3D maps were first generated by stacking a series of 2D layers with the nearest-neighbour interpolation algorithm [22], as illustrated in Fig. 4a. The 3D greyscale map was then processed by image filtering to reduce noise and thresholding to get a binarised image. The threshold value was chosen based on the histogram of the image (Fig. 3c, d). To identify and separate individual particles in 3D dense particle packings, we have employed a watershed-based segmentation technique [23,24], which relies on the fact that eroding the binary image will usually cause contacting features to separate before they disappear. In this study, the method has been extended to 3D space, where full 3D segmentation is performed. Due to memory limitations, the whole 3D image was cut into $350 \times 350 \times 350$ voxel sub-images that were analysed individually, and then restored by numerically combining the different sub-images. The above image processing procedures were performed using Matlab[®] programs along with supplementary libraries such as Matlab image-processing toolbox, DIPimage (The Delft Image Processing Image Processing Toolbox for MATLAB) and Aphelion[®] libraries. The result of the segmentation process in 3D is shown in Fig. 4b and c, in which all uniquely identified objects are rendered using different greyscales.

2.4. Determination of particle size and morphology by SEM

SEM analysis was performed to check the size distributions of all the samples. In order to avoid single particles contacting or agglomerating, a monolayer of dried particles was dispersed homogeneously on a planar substrate, and coated with a thin layer of gold. All analyses were performed using a JEOL JSM-820 Scanning Electron Microscope. Ten samples with approximately 2500 particles were analysed. The 2D images obtained from the SEM observations were digitised and presented to an image analysis program, ImagePro Plus[™]. The analysis program identifies individual particles and recorded information about their morphology. Using SEM, we were able to measure the size accurately; however, this approach only allows the measurement of the projected surface area, diameter or length.

3. Numerical experiments to generate particle packings

We have used DEM simulations to generate numerically packed particle assemblies modelling the particle contacts via the use of force–displacement interactions [25] under the influence of gravity. The DEM algorithm enables the calculation of the positions, velocities and accelerations of all particles by solving Newton's equations of motion, provided the effective force on each particle is known. The effective force on each particle is computed at each iteration by summing the force contributions from inter-particle interactions (via contact force models) and all the external fields that are considered to act on the system. In the “numerical experiments”, spheres were first dropped onto a fixed bed of particles and then allowed to settle under gravity until the average kinetic energy fell below a fraction 10^{-10} of the initial value (*i.e.* the particles came to rest). The 3D simulation cell had identical dimensions along *x*- and *y*-axes (equal to 10 particle diameters) and the height of the cell was used to control the initial packing fraction. Full computational details of the DEM simulations, carried out using a modified version of the DL_POLY code, can be found in Dutt et al. [26].

To ensure that the particle packing numerical experiments were carried out on systems comparable in terms of their size

Table 2
Quantitative information of position, size and shape of objects obtained by image processing on simulated packing of identical hard spheres

Particle index	CMS. X (pixel)	CMS. Y (pixel)	CMS. Z (pixel)	Surface area (pixel ²)	Volume (voxel)	Diameter (pixel)	Sphericity
1	209.80	279.62	32.35	19344	137430	63.92	0.999
2	311.35	152.51	33.94	19336	137413	63.99	0.998
3	379.58	396.72	34.74	19336	137480	63.95	0.999
4	472.45	150.49	35.91	19322	137420	64.03	0.998
5	170.91	226.63	37.36	19332	137445	64.00	0.999
6	290.58	38.77	40.66	19334	137375	63.94	0.998
7	449.67	412.53	40.22	19354	137470	63.95	0.998
8	449.23	210.42	41.96	19320	137431	64.01	0.999
9	129.83	336.66	41.29	19332	137431	63.99	0.997
10	229.32	57.25	43.34	19332	137448	63.97	0.999

distribution to those used in the lab experiments, the XMT scans of the particle size and morphology were used to generate a “packing system” for each sample containing around 2000 particles. In the initial configuration, all the particles were randomly distributed in 3D space with the particles assigned diameters from a size distribution obtained via tomography such that the particles are not in contact with one another. In the DEM simulations, all the particles are assumed to be perfect spheres.

4. Results

Fig. 4 is a schematic of the process of 3D XMT image creation based on a series of 2D reconstructed sections (Fig. 4a) which finally results in all the individual objects being identified (different greyscales as shown in Fig. 4c–d) by the above image processing algorithms. After the segmentation and object finding process, the parameters such as shape, size and position of each individual particle were acquired and all the 3D particles were digitised (Table 1). Before proceeding with further analysis, such as determination of the packing fraction and RDF as described in Section 4.3, the above parameters were verified by comparison with both DEM simulations and experimental data, as described in Sections 4.1 and 4.2, respectively.

4.1. Validation of image processing procedure on ideal DEM particle packings

Simulations were performed to estimate the spatial accuracy of the image processing procedure in the absence of experimental errors. The simulated three-dimensional images were generated by sectioning a packing system generated using DEM, which comprised of hard spheres with identical diameters of 64 pixels (Fig. 5). Each slice had the shape of a square with 512×512 pixels. Those objects that touched boundaries of the image were removed, in order to eliminate finite size effects, and all 130 objects were detected by image processing. The numerical results describing the morphologies of a selection of the spherical particles are shown in Table 2. The mean size of the spheres was measured to be 63.97 ± 0.027 pixels, a deviation less than 0.1% per pixel, which indicated that the image processing phase is almost free of any artefacts for the ideal case of monodisperse spherical particles.

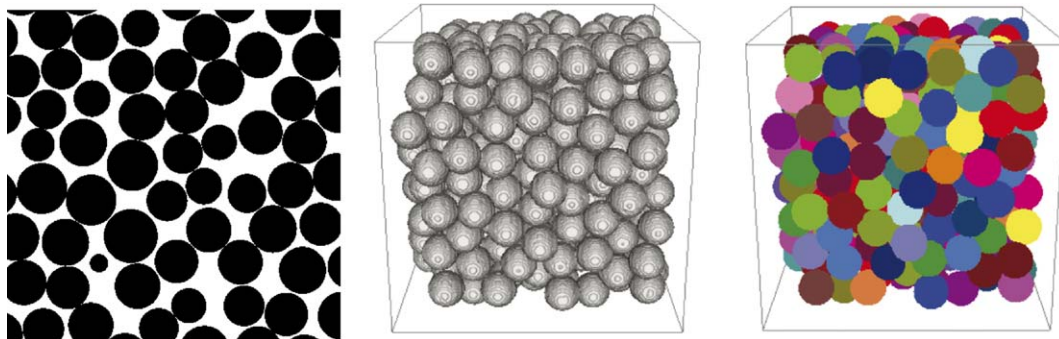


Fig. 5. The morphologies of particles found by image processing procedure. Simulated dataset provided courtesy of Mr. Mark Benedict.

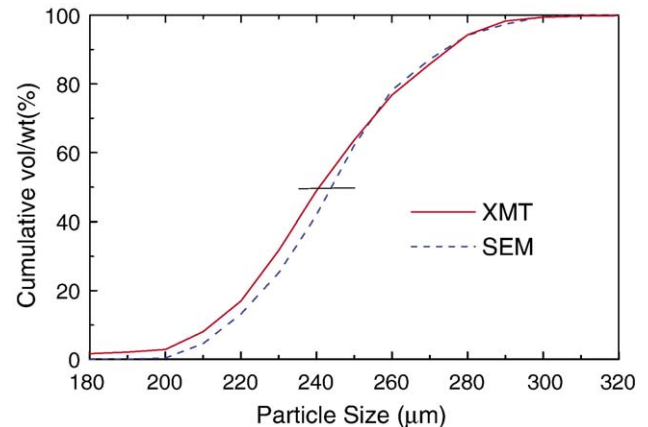


Fig. 6. Comparison of cumulative volumes obtained from SEM and XMT for sample of glass ballotini spheres with particle size of 180–300 μm (shown in Fig. 2a).

4.2. Comparison of particle morphology using SEM

Experimental verification of the XMT measurements was performed by checking the morphologies and size distributions obtained from SEM measurements on the same system. We carried out the validation for a sample of nearly spherical glass spheres but with wide size distribution of 212–300 μm . The packed powder sample was characterised by XMT, and then was dispersed onto a number of planar substrates for SEM analysis. The size of each individual particle was measured, and their cumulative volumes were computed. The morphologies of the glass spheres as determined by XMT, summarized in Table 1, shows that most of the glass beads are highly spherical, in good agreement with the SEM image (Fig. 1) and 2D image analysis. Regarding the size distributions, the cumulative volumes obtained by XMT were found to be in good agreement with those from SEM measurements (Fig. 6). The slight difference between the two curves may arise from some inevitable fracture/breakage in the glass samples, which added extra small particles under XMT measurements. However, the magnitude of the deviation (around 5 μm) is quite low for a system with an average particle size of 240 μm .

4.3. Analytical comparison of packings from experiments and reproductions

We have used packing fraction and RDF measurements to make analytical comparisons between the internal packing

information obtained from XMT scans and DEM simulations. Using the XMT method, the packing fraction can be easily obtained by accumulating all the volume of the identified particles. The packing fractions of monodisperse glass spheres from XMT measurements was $60 \pm 1\%$, which is in good agreement with the numerical (DEM) results (59%) and direct measurements ($60 \pm 3\%$). The above packing fraction calculated from XMT was also in good agreement with that from stereology measurement on reconstructed 2D slices.

The RDF calculations of the particle configurations generated from DEM simulations were compared with those obtained from the XMT measurement (see Fig. 7). The RDF calculations on the configurations of particles were performed as follows: the minimum and maximum inter-particle spacing, r_{\min} and r_{\max} , respectively, were calculated, and the bin width δr was set. The number of total bins, N_{bins} , is then given by $(r_{\max} - r_{\min})/\delta r$. The inter-particle spacing r was calculated between every possible pair of particles, and binned according to the interval in which r lies, as given by $(r_{\min} + i\delta r, r_{\min} + (i+1)\delta r)$, where $i = 1, N_{\text{bins}}$. Finally, each bin is normalized by the volume of a shell with radius $r_{\min} + i\delta r$ and thickness δr , given by $4\pi(r_{\min} + i\delta r)^2 \delta r$. The particles on the boundaries were neglected in both the XMT and DEM data sets to remove the influence of finite size effects. The particle positions and average diameters were used for the RDF calculations.

The RDF calculations of the particle configurations obtained via both the XMT scans and DEM simulations indicate random packing. The RDF had three peaks for inter-particle distances less than or equal $r/\langle D \rangle = 2$. The peaks at $r/\langle D \rangle = 1$ and $r/\langle D \rangle = 2$ represented the nearest-neighbour contacts and those contacts which formed with the particle centres of mass separated by 2 particle diameters, respectively. The presence of the second peak around $\sqrt{3}r/\langle D \rangle$ indicates a degree of local close packing present in the system. The results from the DEM calculations reveal excellent agreement with those from the XMT scans in the case of monodisperse glass spheres (Fig. 7a) and polydisperse glass spheres (Fig. 7b), but only moderately good agreement with those from Celphere system (Fig. 7c).

The RDF calculations can be used to obtain an estimate of the degree of size polydispersity in a sample by the broadening of the distinct peaks observed for RDF calculations of monodisperse particle packing (Fig. 7a). The size distribution of the particles in the polydisperse glass bead sample demonstrates the degree of size polydispersity, which is responsible for the lack of distinct peaks at the second and third nearest-neighbour distances (Fig. 7b). In the case of Celphere, the peak at first contact is significantly reduced in height and broadened in comparison to the DEM model results, although the second and third nearest-neighbour peaks are relatively similar. This is due to the assumption of perfect sphericity of the particles in the DEM model, which results in a much smaller range of inter-particle distances at $r/\langle D \rangle \approx 1$. However, the peaks at second and third nearest-neighbour distances are relatively unaffected by the assumption of sphericity, which could indicate that the orientation of the particles are uncorrelated over such distances. For more highly aspherical systems, it would be necessary to characterise the orientation as well as the position of the

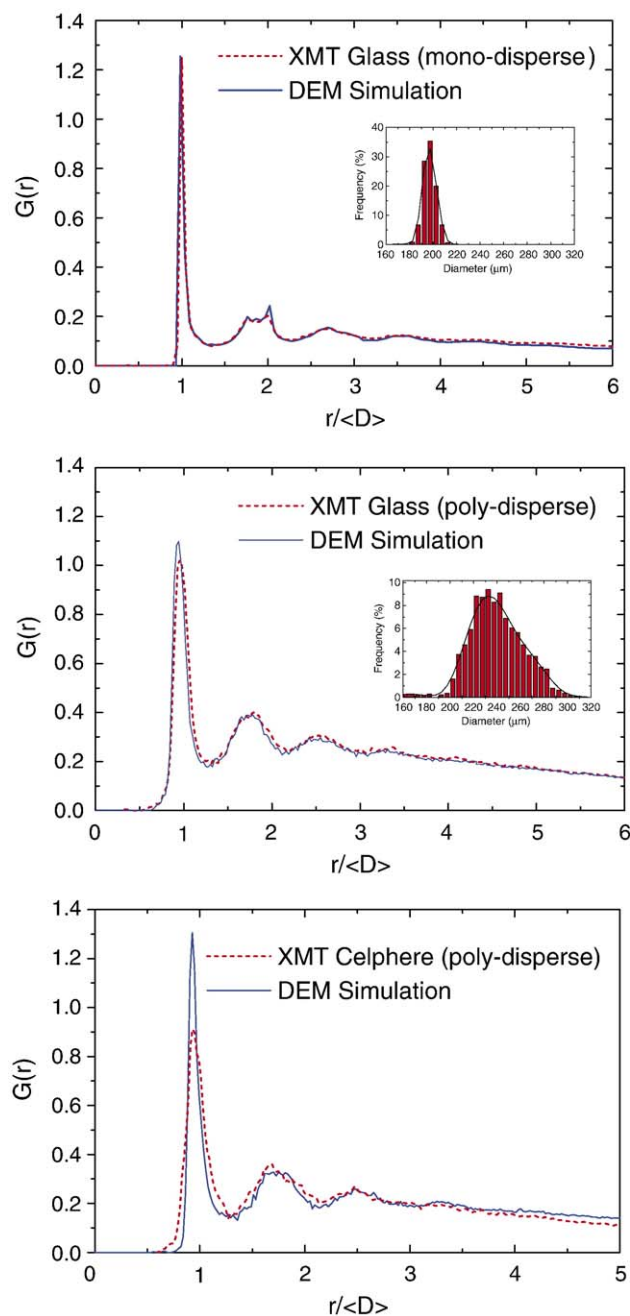


Fig. 7. Comparison of the RDFs of the monodisperse glass packing structure, polydisperse glass and Celphere packing structure obtained from XMT (solid curve) and DEM simulation (dashed curve).

particles, and this information is available in principle from XMT.

5. Conclusions

The 3D maps of the internal structure of dense random packings representative of pharmaceutical systems have been obtained quantitatively and non-destructively by XMT, using image processing routines. This method enabled the particle size and shape distributions for mono- and polydisperse mixtures of spherical particles to be determined, with results that are

consistent with 3D simulation images and SEM analysis of the 2D samples of the powders, indicating that the XMT data is likely to be free of any artefacts introduced during the image processing phase. A DEM model for the powder packing was successfully produced based on individual particle information obtained from XMT. The RDFs calculated by DEM were in quantitative agreement with those obtained from XMT for mixtures of spherical particles. This model-based approach could be used in other problems such as powder compaction or shear. In conclusion, the methodology we have described represents a novel method of linking the internal packing structure of particle agglomerates generated in laboratory and numerical experiments, and thus approach can be extended to a variety of systems consisting of particles of different shape and size. We are currently using this technique to explore a multitude of powder systems of greater relative particle complexity, in which the shape information such as sphericity and aspect ratio will be incorporated.

Acknowledgements

This work was supported financially by Pfizer Ltd. We also thank Dr. Georgina E. Milroy and other members of the Pfizer Institute for Pharmaceutical Materials Science in Cambridge for their valuable suggestions and discussions.

References

- [1] X. Jia, R.A. Williams, A packing algorithm for particles of arbitrary shapes, *Powder Technology* 120 (2001) 175–186.
- [2] G.E. Mueller, Numerically packing spheres in cylinders, *Powder Technology* 159 (2005) 105–110.
- [3] W.I. Salvat, N.J. Mariani, G.F. Barreto, O.M. Martinez, An algorithm to simulate packing structure in cylindrical containers, *Catalysis Today* 107–108 (2005) 513–519.
- [4] G.D. Scott, Packing of equal spheres, *Nature* 188 (1960) 908–909.
- [5] G.D. Scott, D.M. Kilgour, The density of random close packing of spheres, *Journal of Physics. D, Applied Physics* 2 (1969) 863–866.
- [6] G.E. Mueller, Radial void fraction distributions in randomly packed tied beds of uniformly sized spheres in cylindrical containers, *Powder Technology* 72 (1992) 269–275.
- [7] G.E. Mueller, Angular void fraction distributions in randomly packed fixed beds of uniformly sized spheres in cylindrical containers, *Powder Technology* 77 (1993) 313–319.
- [8] W.K. Kegel, A. van Blaaderen, Direct observation of dynamical heterogeneities in colloidal hard-sphere suspensions, *Science* 287 (2000) 290–293.
- [9] E.H.C. Bromley, I. Hopkinson, Confocal microscopy of a dense particle system, *Journal of Colloid and Interface Science* 245 (2002) 75–80.
- [10] E.E. Ehrichs, H.M. Jaeger, G.S. Karczmar, J.B. Knight, Kuperman V. Yu, S.R. Nagel, Granular convection observed by magnetic-resonance-imaging, *Science* 267 (1995) 1632–1634.
- [11] T. Shinbrot, A. Alexander, F.J. Muzzio, Spontaneous chaotic granular mixing, *Nature* 397 (1999) 675–678.
- [12] W. Man, A. Donev, F.H. Stillinger, M.T. Sullivan, W.B. Russel, D. Heeger, S. Inati, S. Torquato, P.M. Chaikin, Experiments on random packings of ellipsoids, *Physical Review Letters* 94 (19) (2005) 198001.
- [13] G.T. Seidler, G. Martinez, L.H. Seeley, K.H. Kim, E.A. Behne, S. Zaranek, B.D. Chapman, S.M. Heald, D.L. Brewre, Granule-by-granule reconstruction of a sandpile from X-ray microtomography data, *Physical Review E* 62 (2000) 8175–8181.
- [14] P. Richard, P. Philippe, F. Barbe, S. Bourles, X. Thibault, D. Bideau, Analysis by X-ray microtomography of a granular packing undergoing compaction, *Physical Review E* 68 (2003) 020301.
- [15] R.A. Williams, X. Jia, Tomographic imaging of particulate system, *Advanced Powder Technology* 14 (2003) 1–16.
- [16] T. Aste, M. Saadatfar, A. Sakellariou, T.J. Senden, Investigating the geometrical structure of disordered sphere packings, *Physica A Statistical Mechanics and its Applications* 339 (1–2) (2004) 16–23.
- [17] D. Golchert, R. Moreno, M. Ghadiri, J. Litster, Effect of granular morphology on breakage behaviour during compression, *Powder Technology* 143–144 (2004) 84–96.
- [18] G.T. Herman, *Image Reconstructions from Projections: The Fundamentals of Computerized Tomography*, Academic Press, New York, 1980.
- [19] S.R. Stock, X-ray microtomography of materials, *International Materials Reviews* 44 (1999) 141–164.
- [20] M.E. Aulton, *Pharmaceutics: The Science of Dosage Form Design*, 2nd ed., Churchill Livingstone, London, 2002.
- [21] http://www.skyscan.be/next/spec_1172.htm.
- [22] G. Herman, C. Coin, The use of 3D computer display in the study of disk disease, *Journal of Computer Assisted Tomography* 4 (1980) 564–567.
- [23] S. Beucher, C. Lantuejoul, Use of watersheds in contour detection, *Proc. International Workshop on Image Processing: Real-Time Edge and Motion Detection/Estimation*, Rennes, United States, 1979, pp. 17–21.
- [24] J.C. Russ, *The Image Processing Handbook*, 2nd ed., Boca Raton, London, 1995.
- [25] P.A. Cundall, O.D.L. Strack, A discrete numerical model for granular assemblies, *Geotechnique* 29 (1979) 47–65.
- [26] M. Dutt, B.C. Hancock, A.C. Bentham, J.A. Elliott, An implementation of granular dynamics for simulating frictional elastic particles based on the DL-POLY code, *Computer Physics Communications* 166 (2005) 26–44.